Polymer Chemistry

PAPER

View Article Online
View Journal | View Issue



Cite this: *Polym. Chem.*, 2015, **6**, 7550

# The effect of molecular geometry on the polymer/fullerene ratio in polymer solar cells†

Jianyu Yuan, Yu Liu, Huilong Dong, Xiaobo Shi, Zeke Liu, Youyong Li and Wanli Ma*

Received 10th June 2015,
Accepted 31st August 2015

DOI: 10.1039/c5py00893j

www.rsc.org/polymers

In order to reveal the correlation between molecular structures and the corresponding film morphology as well as polymer/fullerene blend ratio, a new donor–acceptor (D–A) polymer poly-(benzodithiophene-naphthothiophenedione) (**PTN8**) based on and was synthesized, which was intentionally designed to further increase the molecular structure bulkiness of our previously reported polymer poly-(benzodithiophene-thienopyrroledione) (**PTP8**). The experimental results and theoretical calculations indicate that both polymers have similar solubilities, optical properties and energy levels, while the structural modification has a significant impact on the polymer intermolecular packing and crystallinity by altering the backbone coplanarity. The different molecular geometries lead to significantly different device performances, optimal fullerene loadings and efficiency dependence on blend ratios. Therefore molecular geometry should be carefully considered when rationally designing polymers for reducing the use of fullerene.

## Introduction

Solution-processed flexible polymer solar cells (PSCs) have attracted tremendous interest in both academia and industry during the past two decades.[1] Great efforts have been devoted to molecular design, synthesis, and the processing of bulk hetero-junction (BHJ) devices, leading to a high efficiency over 10%.[2] However, the device performance is still low compared with its inorganic counterparts. The relatively low short-circuit current ($J_{sc}$) and fill factor (FF) of PSCs are mainly limited by the charge carrier mobility of the polymer and polymer/phenyl-$C_{71}$-butyric acid methyl ester ($PC_{71}BM$) blend morphology.[3] In general, an ideal percolated network constructed by polymer/$PC_{71}BM$ with an optimized blend ratio is considered essential for efficient charge transport.[4] Both film mobility and morphology can be very sensitive to the blend ratio. According to a variety of highly efficient polymer/fullerene BHJ solar cells reported previously, we found that some systems were optimized with a D/A blend ratio around 1/1 by weight, while most of them had optimal blend ratios between 1/1 and 1/4.[5] Recently, McGehee *et al.* revealed that the fullerene intercalation into flexible polymer side-chains may be responsible for the optimal blend ratio.[6] And our latest report proved that dense polymer side-chains can prevent fullerene intercalation and result in a low optimal fullerene loading.[7] As is well-known, $PC_{71}BM$ shows an apparently weaker extinction coefficient in the visible region than conjugated polymers.[8] Thus larger film thickness is required to absorb enough light for devices with a high fullerene ratio, which will, however, result in increased recombination and fill factor (FF) degradation.[9] In addition, $PC_{71}BM$ tends to aggregate at elevated temperatures, causing thermal instability for PSCs. Therefore, the reduction of fullerene use in PSCs may be a useful strategy to improve the device efficiency and thermal stability. In our previous work, the D/A ratio can be adjusted by tailoring the polymer side-chains.[7b] With double aromatic side-chains, polymer **PTP8** can achieve high performance at very low fullerene loadings due to its high side-chain density. However, as shown in Scheme 1, the dihedral angle always exists for single

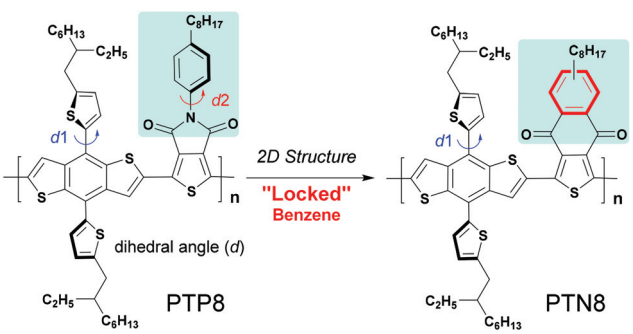


**Scheme 1** Chemical structure of **PTP8** and **PTN8**.

*Institute of Functional Nano & Soft Materials (FUNSOM), Jiangsu Key Laboratory for Carbon-Based Functional Materials & Devices, Collaborative Innovation Center of Suzhou Nano Science and Technology, Soochow University, 199 Ren-Ai Road, Suzhou Industrial Park, Suzhou, Jiangsu 215123, P. R. China. E-mail: wlma@suda.edu.cn*

†Electronic supplementary information (ESI) available. See DOI: 10.1039/c5py00893j

bonded 2-dimensional alkyl aromatic side-chains, indicating a certain extent of flexibility. If the polymer side-chain can be designed more stiff, it is very likely that the intercalation of the fullerene will be further prevented. Inspired by this hypothesis, we were encouraged to further investigate the side-chain steric effect by introducing the locked benzene ring. A classical organic monomer naphtho[2,3-*c*]thiophene-4,9-dione (NTDO) exhibits similar optical and electrical properties to thieno[3,4-*c*]-pyrrole-4,6-dione.[10] By using the Stille polycondensation reaction,[11] a new polymer **PTN8** was successfully prepared to further study the correlation between molecular structure and polymer/fullerene blend ratio. According to the theoretical simulation and grazing incidence X-ray diffraction (GIXD) results, **PTP8** and **PTN8** demonstrate quite different molecular geometries and crystallinities, while showing similar optical and electrical properties. The efficiency dependence on the polymer/$PC_{71}BM$ blend ratio is quite different for these two polymers with a high polymer/fullerene blend ratio. The discrepancy can mainly be attributed to their distinctly different molecular geometries, which has a profound influence on polymer inter-chain packing, crystallinity, morphology and hence device performance. Therefore molecular geometry should be carefully considered when rationally designing a polymer for reducing the use of fullerene.

## Results and discussion

### Synthesis and characterization

The desired polymer **PTN8** was synthesized *via* Stille polymerization using a distannylated BDT monomer (**1**) and a dibrominated NTDO monomer (**2**) which was similar to **PTP8** (Scheme 2).[7b] After the reaction, the reaction mixture was cooled to room temperature and the polymer was precipitated in methanol, filtered, and was then subjected to Soxhlet extraction with methanol and hexane to remove the impurities and oligomers. The remaining crude product in the thimble was then extracted with chloroform, and precipitated into methanol. The number-average molecular weight ($M_n$) and dispersity ($Đ$) were determined by gel permeation chromatography (GPC). **PTP8** has a $M_n$ of 23.5 kDa and a $Đ$ of 2.38, while **PTN8** has a $M_n$ = 20.3 kDa and a $Đ$ = 2.17. Both **PTP8** and **PTN8** exhibit excellent solubility in commonly used organic solvents at room temperature, including chloroform (CF), chlorobenzene (CB) and *o*-dichlorobenzene (ODCB).

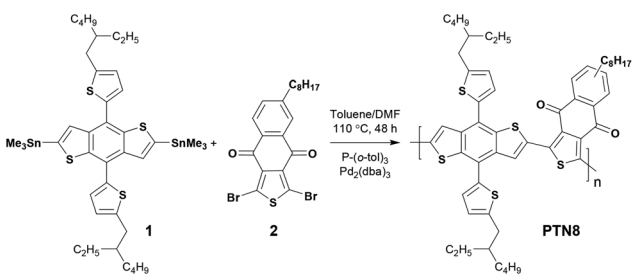


Scheme 2 The synthetic route to **PTN8**.

### Optical and electrochemical properties

UV-vis absorption spectra of **PTP8** and **PTN8** in dilute chloroform solution and in thin films cast from chloroform are shown in Fig. 1, with the corresponding data summarized in Table 1. Both polymers show similar absorption from 300 to 700 nm due to the relatively weak electron withdrawal ability of TPD and NTDO. The red shift between the absorption maximum in solution and in the film state is ~10 nm. We noted that **PTP8** exhibits an additional absorption peak at ~627 nm compared with **PTN8**, which could be attributed to the stronger π–π interaction between polymer backbones,[12] indicating a better coplanar configuration for **PTP8**. Judging from the absorption edges of polymer films, the corresponding optical band-gaps ($E_g^{opt}$) of the two polymers were calculated as 1.78 eV (**PTP8**) and 1.79 eV (**PTN8**), respectively. As measured by cyclic voltammetry (CV, Fig. 2), the highest occupied molecular orbital (HOMO) and lowest unoccupied molecular orbital (LUMO) energy levels of **PTN8**, calculated from the onset potential of the first oxidation and reduction peaks, are −5.60 eV and −3.55 eV respectively, which are quite similar to those of **PTP8**.[7b] In summary, **PTP8** and **PTN8** show similar optical band-gap and energy levels after the structural modification.

### Theoretical calculations

To obtain the structural and electronic properties of **PTP8** and **PTN8**, density functional theory (DFT) calculations were performed by using the DMol3[13] program. The all-electron generalized gradient approximation functional by B88 exchange and LYP correlation[14] (GGA-BLYP), along with a double numerical plus polarization (DNP) basis set, was used in calculations on monomers. While the solvent effect[15] (chloroform, $\varepsilon$ = 4.806) was also taken into consideration to fit the actual conditions. Then we carried out molecular mechanic simulations to

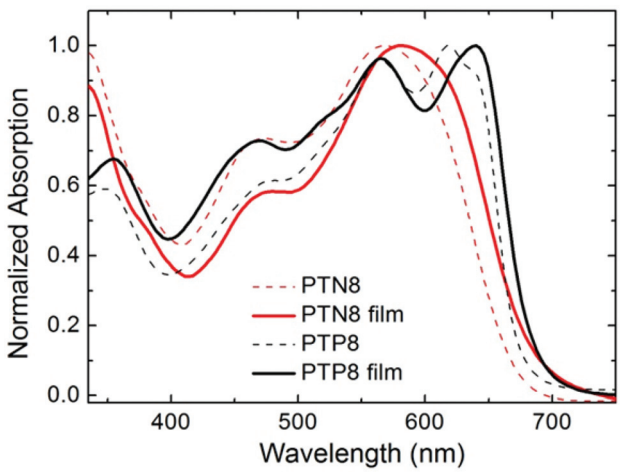


Fig. 1 Normalized UV-vis absorption spectra of **PTP8** and **PTN8** in dilute chloroform solution and thin films spin-cast from chloroform.

Table 1 Optical and electrochemical properties of the polymers

| Polymer | $\lambda_{max}$ [nm] Solution | $\lambda_{max}$ [nm] Film | $\lambda_{onset}$ [nm] Film | $E_g^{opt\,a}$ [eV] | HOMO [eV] | LUMO [eV] | HOMO$^{cal}$ [eV] | LUMO$^{cal}$ [eV] |
|---|---|---|---|---|---|---|---|---|
| **PTP8** | 565, 614 | 565, 640 | 695 | 1.78 | −5.59 | −3.62 | −4.69 | −3.35 |
| **PTN8** | 568 | 582 | 690 | 1.79 | −5.60 | −3.55 | −4.70 | −3.25 |

[a] $E_g^{opt}$ is determined by the absorption onset of polymers as thin films, $E_g^{opt} = 1240/\lambda_{onset}$.

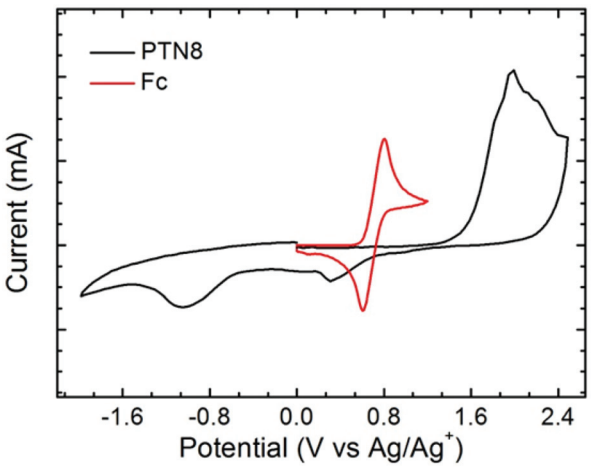


Fig. 2 Cyclic voltammetry curves of PTN8 (black) tested in $CH_3CN$ (the polymer film is deposited on the glassy carbon electrode).

compare the structural geometry of the polymers by using the Forcite program. We choose $n$ = 5 to stand for the polymers, and the structures were constructed based on atactic polymerization. The Dreiding force field[16] was used for the calculations.

The geometries of **PTP8** and **PTN8** are shown in Fig. 3. According to the simulation results, the incorporation of NTDO induces great changes in the polymer backbone geometry. The backbones of the molecules are aligned to the *XZ* plane to minimize the summation of *Y* coordinates of each atom. The calculated standard deviations of *Y* coordinates of each atom are defined as Y_StDev. According to the result, the Y_StDev value of **PTN8** (3.952) is evidently larger than that of **PTP8** (1.483), indicating that the co-planarity of the former is indeed getting worse by the incorporation of "locked benzene". It is worth noting that PTN8′ has quite similar backbone geometries and energy levels with PTN8. Thus we believe that the structural difference of side-chains has a minimal effect on the corresponding polymer properties. Furthermore, we use 2d GIXD to probe the practical molecular packing (Fig. 3) in the solid state. We can clearly observe the (010) peak in the out of plane direction for PTP8, which indicates strong π–π stacking and face-on orientation. In comparison, no apparent peaks can be observed in the 2d XRD spectrum for PTN8, indicating its amorphous nature. This observation is well consistent with our theoretical results. As shown in Fig. 4, the distance between S–O atoms in **PTN8** with different chemical structures (2.708 Å and 2.668 Å) is shorter than that in **PTP8** (3.006 Å), which leads to a more twisted structure (larger dihedral angle) to balance the molecular interaction and therefore worse co-planarity for **PTN8**. By combining the simulation and experimental results, we revealed the detailed geometry changes after introducing "locked benzene".

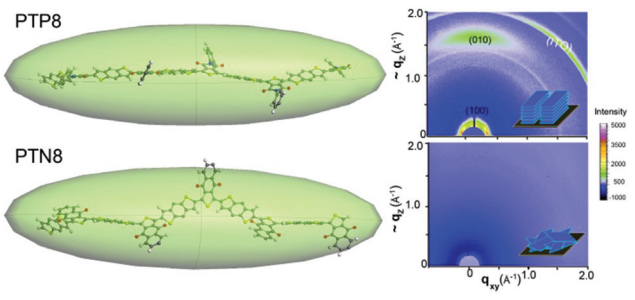


Fig. 3 Calculated 3D steric arrangement of the pentamer backbones and 2d GIXD images for **PTP8** and **PTN8**, respectively.

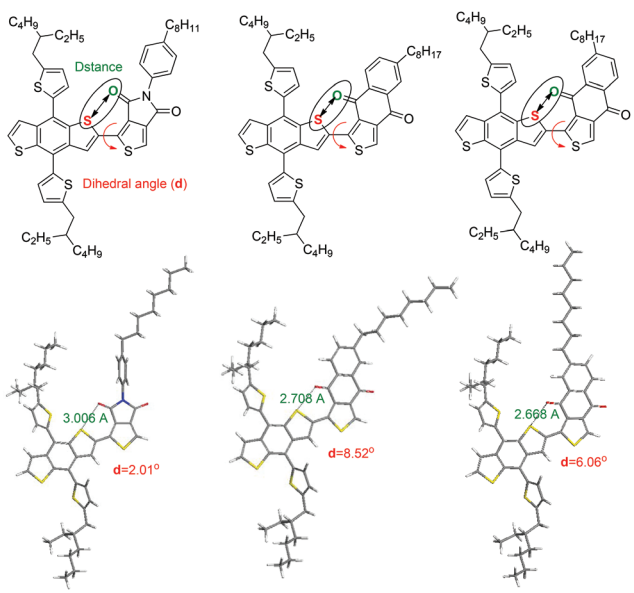


Fig. 4 Optimized geometries of **PTP8**, **PTN8** and **PTN8′**.

### Photovoltaic performance

Bulk hetero-junction PSCs were fabricated using a polymer and $PC_{71}BM$ with a conventional device structure of ITO/PEDOT:PSS(40 nm)/polymer:$PC_{71}BM$/LiF(0.6 nm)/Al(100 nm). Throughout the experiment, a fixed polymer concentration of 8 mg $mL^{-1}$ was used. 1,8-Diiodooctane (DIO) was used as an solvent additive to improve the film morphology, which has been extensively studied in previous work in PSCs.[17] The introduction of alkyl aromatic side-chains to both D/A monomers may become a general approach in molecular design to effectively prevent the intercalation of fullerene into polymer side-chains, leading to the reduced use of $PC_{71}BM$ and additives. In this work, we try to further reduce the intercalation by the introduction of "locked benzene". Thus the device performance of the PSCs based on **PTN8**:$PC_{71}BM$ was investigated. The *J–V* characteristics of the optimized devices with different blend ratios are shown in Fig. 5a with the detailed parameters listed in Table 2.

All the devices exhibit remarkably high $V_{oc}$ of around 1.00 V. And PCEs of 3.17%, 3.51%, 3.24%, 2.83% 2.39% and 1.16% are achieved at the weight ratios of 1 : 1, 1 : 0.8, 1 : 0.7, 1 : 0.6, 1 : 0.5 and 1 : 0.3, respectively. The device performance is relatively lower than that of **PTP8**. In addition, the efficiency is more sensitive to the blend ratio, as shown in Fig. 5b. External quantum efficiencies (EQE) of optimized **PTN8** devices with different blend ratios were measured and shown in Fig. 6, The devices show a relatively high photo-conversion efficiency over the whole wavelength range (300–700 nm). The $J_{sc}$ calculated by integrating the EQE curve (Fig. 6) with an AM 1.5G reference spectrum is ~10% higher than the corresponding $J_{sc}$ obtained from the *J–V* curves, which may be due to stronger charge recombination at higher light intensities for the **PTN8**/$PC_{71}BM$ blend.[18]

We originally expect that **PTN8** with "locked benzene" should show enhanced molecular π-stacking and carrier transporting, which can further improve film absorption and charge transport in photovoltaic devices. All these results don't quite meet our expectations for the intentionally designed polymer structure. But we have noted that the optimal blend ratio is indeed decreased to 1 : 0.8, compared with 1 : 1 for **PTP8**[7b] without the "locked benzene". Thus the modified structure shows certain contributions to reduce the $PC_{71}BM$ percentage in the polymer/$PC_{71}BM$ blend of PSCs. Compared with **PTP8**, **PTN8** seems less effective in preventing the fullerene intercalation. We speculate that the more twisted polymer backbone of **PTN8** (Fig. 4) may actually increase the side-chain

Table 2 Photovoltaic characteristics of PSCs based on **PTN8**/$PC_{71}BM$ blends with different D/A weight ratios under a simulated AM 1.5G illumination (100 mW $cm^{-2}$)

| D/A ratio | $V_{oc}$ [a] [V] | $J_{sc}$ [a] [mA $cm^{-2}$] | $J_{sc\ cal}$ | FF[a] [%] | PCE[a] [%] |
|---|---|---|---|---|---|
| 1 : 1.0 | 0.96 ± 0.00 | 8.07 ± 0.25 | 9.19 | 37.5 ± 2.1 | 2.91 ± 0.26 |
| 1 : 0.8 | 0.97 ± 0.01 | 8.28 ± 0.14 | 9.47 | 41.7 ± 1.0 | 3.35 ± 0.16 |
| 1 : 0.7 | 0.97 ± 0.01 | 7.79 ± 0.23 | 8.70 | 40.3 ± 1.2 | 3.06 ± 0.15 |
| 1 : 0.6 | 0.98 ± 0.01 | 7.12 ± 0.10 | 7.89 | 38.7 ± 1.8 | 2.70 ± 0.13 |
| 1 : 0.5 | 1.02 ± 0.00 | 6.43 ± 0.20 | 7.26 | 34.5 ± 0.9 | 2.27 ± 0.12 |
| 1 : 0.3 | 1.03 ± 0.01 | 3.76 ± 0.05 | 4.27 | 28.7 ± 0.6 | 1.11 ± 0.05 |

[a] Average number based on 6 devices.

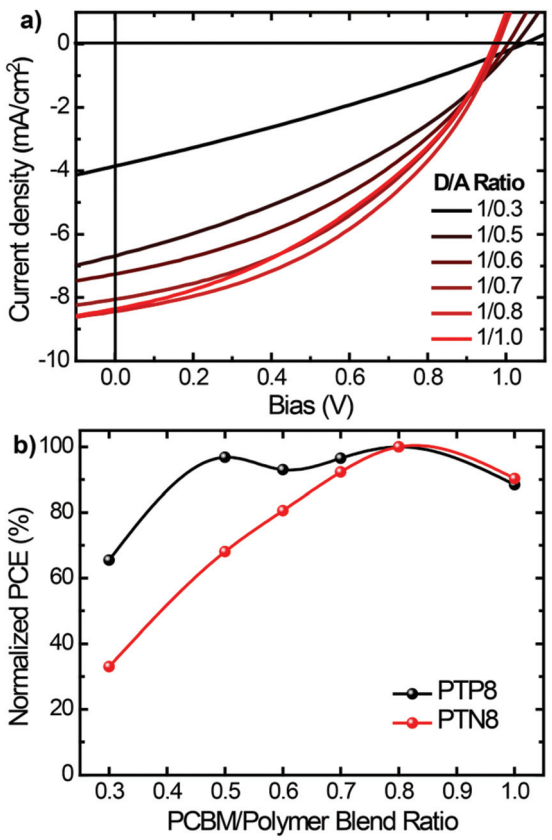


Fig. 5 (a) *J–V* curves of optimized PSCs based on **PTN8**:$PC_{71}BM$ with different blend ratios; (b) efficiency dependence on polymer/$PC_{71}BM$ weight ratios for device based on **PTP8** and **PTN8**.

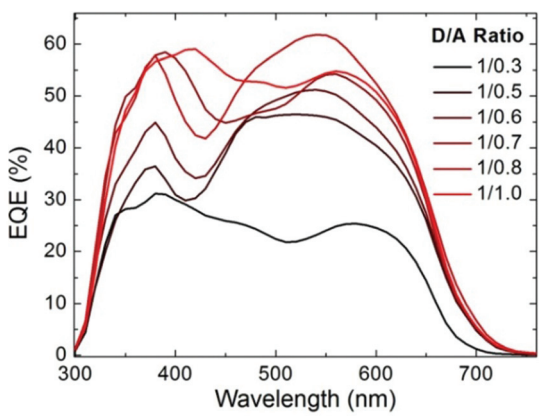


Fig. 6 EQE of **PTN8**/$PC_{71}BM$ based solar cells with different polymers to fullerene w/w ratios.

space and thus benefit intercalation. Meanwhile, the reduced inter-chain packing (Fig. 3) of the modified polymer may allow the fullerene to diffuse into the polymer matrix more easily. Therefore, it is not surprising to see that more planar **PTP8** exhibit lower optimal fullerene loading. The decreased device performance was mainly due to the reduced $J_{sc}$ and FF, which is very likely related to the film absorbance, charge dissociation and transport process.

We further investigated the optical properties of the polymer/$PC_{71}BM$ blend film. As shown in Fig. 7, the optical absorption of the **PTN8**/fullerene layer is evidently stronger than that of **PTP8**/fullerene, which is not consistent with their photo current. We then investigated the photoluminescence (PL) quenching efficiency of blend films PTP8/$PC_{71}BM$ and PTN8/$PC_{71}BM$ with different D/A ratios, as shown in Fig. 8a. We can observe that the PL of **PTN8** neat film is effectively quenched when blended with two different percentage

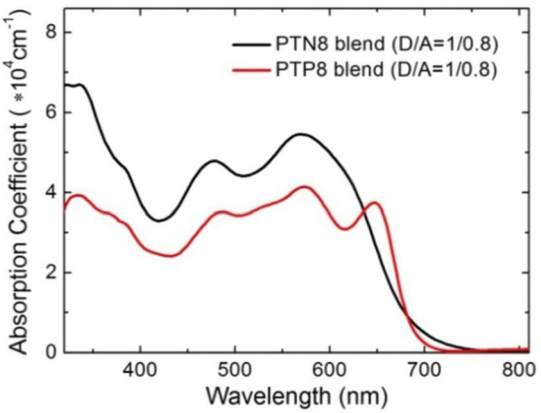


**Fig. 7** UV-vis absorption spectra of **PTP8**/$PC_{71}BM$ and **PTN8**/$PC_{71}BM$ blends cast from chloroform with optimal additive (1.5% DIO, v/v) content at the same D/A ratio of 1/0.8.

$PC_{71}BM$ contents. The PTP8/$PC_{71}BM$ blend film demonstrates similar polymer PL quenching which suggests that an efficient photoinduced charge separation occurs in the fullerene/polymer blends. To confirm this result, we further conducted transient state fluorescence measurements to compare the exciton dissociation efficiency for the two blend films. As shown in Fig. 8b, the PL lifetime of PTP8/$PC_{71}BM$ and PTN8/$PC_{71}BM$ is similar, which is consistent with the results shown in Fig. 8a. Therefore as a result, the comparison of PL quenching for the two polymers can hardly account for the difference in their device photocurrent.

## Blend film morphology

Thus we systematically studied their morphology to locate the possible factors for reduced device performance. The effects of polymer molecular geometry and blend ratio on film morphology were investigated by using AFM and TEM. AFM topography images (Fig. 9) were collected on films cast from **PTN8**:$PC_{71}BM$ solution with optimal amounts of additives. Interestingly, the **PTN8** blend demonstrates a smooth morphology over a wide range of weight ratios, quite different from the "valley-like" domains with varied sizes in the **PTP8** blend[7b] (see the ESI, Fig. S4†). The observations suggest that the film is rather amorphous, which is in accordance with its XRD spectra (Fig. 3). Moreover, the morphology change with processing additives is less pronounced for **PTN8**. It is well known that the forming of continuous and crystalline carrier paths is crucial to the charge mobility and device performance.[3,4] The amorphous blend film of **PTN8** suggests that the crystallinity of both polymer and fullerene is low. In contrast, the valley-structures in the **PTP8** blend film were confirmed to be highly crystalline $PC_{71}BM$-rich clusters.[7b] Thus it is plausible that the devices based on **PTP8** have better charge transport and higher performance.

In order to confirm the AFM results, TEM experiments (Fig. 10) were also carried out to investigate the bulk mor-

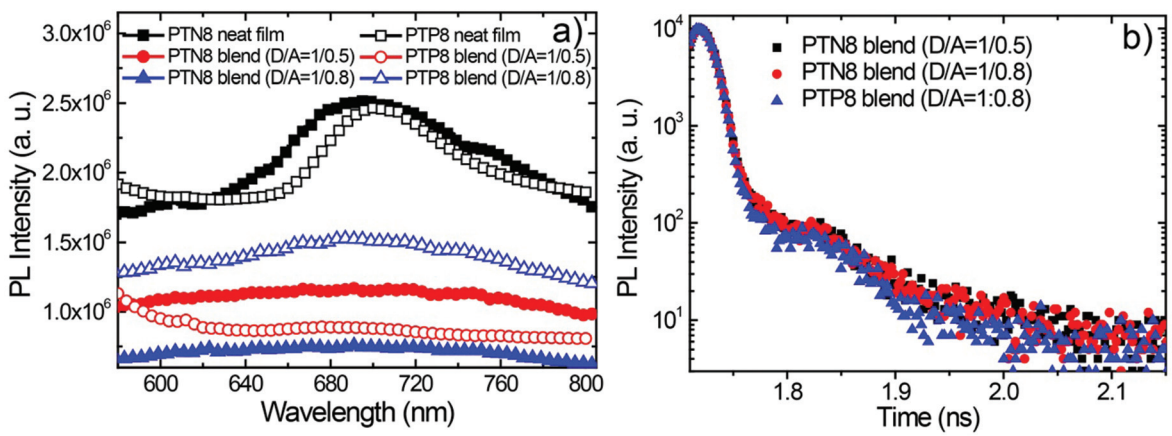


**Fig. 8** (a) Photoluminescence spectra of **PTN8**, **PTP8** neat film and polymer/$PC_{71}BM$ blend films with D/A ratios of 1 : 0.5 and 1 : 0.8; (b) photoluminescence decay profiles of the films based on **PTN8**/$PC_{71}BM$ and **PTP8**/$PC_{71}BM$ blends.

 

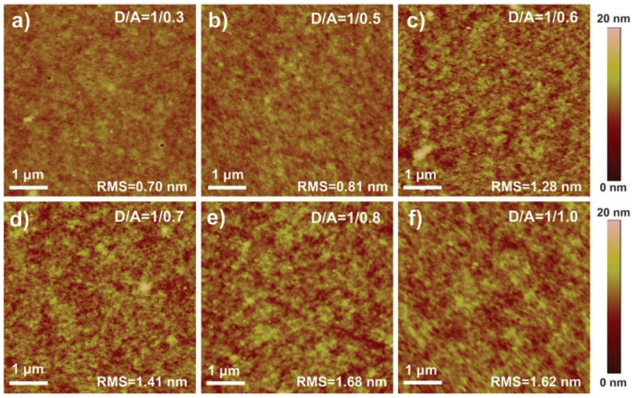


**Fig. 9** (a–f) AFM height images of **PTN8**:$PC_{71}BM$ blend films with different D/A ratios cast from chloroform with and without DIO additive (concentrations are given in the Experimental section).

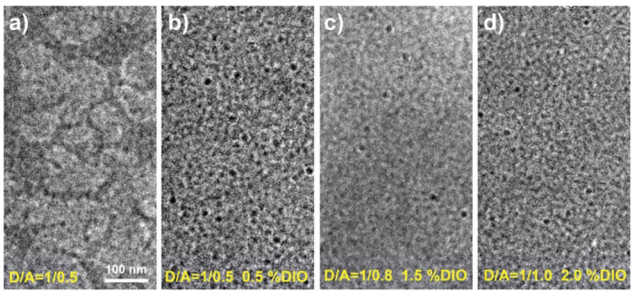


**Fig. 10** (a–d) TEM images of **PTN8**:$PC_{71}BM$ blend films with different D/A ratios cast from chloroform with and without DIO additive (concentrations are given in the Experimental section).

phology of the **PTN8**:$PC_{71}BM$ blend under varied processing conditions. We can observe huge polymer-rich and $PC_{71}BM$-rich domains in the **PTN8**-based blend cast from pure chloroform. After the addition of an additive DIO, a much finer phase separation is demonstrated. With increased blend ratio, the blend morphology doesn't show a significant difference. The detailed morphology of the film was further investigated by high-resolution high angle annular dark field scanning transmission electron microscopy (HAADF-STEM). As shown in Fig. S5,† the phase separation of the two blend films can be more clearly observed. We noted that the domain sizes in the **PTN8** blend are on the micro-meter scale, which is far from the optimal conditions for phase segregation. In contrast, in the **PTP8** blend film, the demixing of polymer/fullerene is much finer and polymer nano-fibers can be observed (Fig. S5a†). The ideal nano-fiber structure will increase diffusional escape probability for mobile charge carriers, and hence decrease recombination.[4] Compared with **PTP8**, no similar polymer nano-fibers in **PTN8** can be observed. The morphology discrepancy can be attributed to the different coplanarities and crystallinities of the two polymers, as a result of different molecular geometries.

# Conclusions

In order to reduce the $PC_{71}BM$ percentage in the polymer/$PC_{71}BM$ blend of PSCs, a new polymer **PTN8** was synthesized by modifying the previously reported **PTP8** with high side-chain density. Their optical properties, molecular geometry, device performance and film morphology were systematically investigated and compared. Both polymers exhibited similar optical properties while **PTP8** has lower optimal fullerene loading and its performance is less sensitive to the fullerene ratio. The discrepancy can mainly be attributed to their distinctly different molecular geometries, which has a profound influence on polymer inter-chain packing, crystallinity, morphology and hence device performance. In general, we revealed that in PSCs, polymer side-chain density is not the only factor determining the polymer/fullerene ratio, but the polymer molecular geometry can also play a very important role, which should be carefully considered for rational polymer design.

# Experimental

### Materials and instruments

All reactions and manipulations were carried out under an argon atmosphere with the use of standard Schlenk techniques. All chemicals were purchased from Sigma-Aldrich and used as received, unless stated otherwise. Toluene, THF and DMF were purchased from Adamas Reagent, dried over sodium/benzophenone and distilled before using. DMF was distilled over $CaH_2$. Chloroform, methanol and dichloromethane were used as received from Adamas Reagent. PEDOT:PSS (Clevios™ P VP Al 4083, filtered at 0.45 μm) used for the fabrication of PSCs was purchased from Heraeus. Phenyl-$C_{71}$-butyric acid methyl ester ($PC_{71}BM$, purity 99%) was purchased from American Dye Source (Canada). The distannylated BDT monomer 2,6-bis(trimethyl-tin)-4,8-bis(5-(2-ethylhexyl)-thiophen-2-yl)benzo[1,2-*b*:4,5-*b*′]di-thiophene (**1**) was prepared according to the literature.[7a] The dibrominated NTDO monomer 1,3-dibromo-6-hexylnaphtho[2,3-*c*]thiophene-4,9-dione (**2**) was prepared according to Prof. Li's method.[10b] The polymer **PTP8** was obtained according to our reported procedure.[7b] The $M_n$ of **PTP8** was measured as 23.5 kDa with a PDI = 2.38 using THF as the eluent at 40 °C.

$^1H$ NMR data were recorded at room temperature on a Varian Unity Inova 400 MHz spectrometer in $CDCl_3$ using tetramethylsilane [$(CH_3)_4Si$; $\delta$ = 0.00 ppm] as an internal standard. GC-MS spectra were obtained by using a ThermoFisher Scientific GC/MS Trace-ISQ mass spectrometer. The weight-average molecular weight $M_w$, and polydispersity index (PDI; given by $M_w/M_n$, where $M_n$ is the number-average molecular weight) of the polymers were determined against a polystyrene standard by gel permeation chromatography (GPC) on a PL-GPC 50 apparatus, and THF was used as the eluent at a flow rate of 1.0 mL $min^{-1}$ at 40 °C. UV-vis-NIR spectra were recorded on a Perkin Elmer model Lambda 750 instrument. Cyclic voltammetry (CV) measurements were conducted using

a standard three-electrode configuration under an argon atmosphere. A three-electrode cell equipped with a glassy carbon working electrode, an Ag wire reference electrode and a Pt wire counter-electrode. The measurements were performed in absolute acetonitrile with tetrabutylammonium hexafluorophosphate (0.1 M) as the supporting electrolyte at a scan rate of 100 mV $s^{-1}$. Polymer films for CV test were drop-casted onto the glassy carbon working electrode from a 5 mg $mL^{-1}$ chloroform solution. The absolute energy level of ferrocene/ferrocenium ($Fc/Fc^{+}$) was found to be 4.8 eV under vacuum. Photoluminescence spectra were recorded on a Horiba Jobin Yvon model FL-TCSPC, the neat polymer was spin cast from chloroform solutions with a concentration of 10 mg $mL^{-1}$, the thickness was 100 nm for **PTP8**, and 75 nm for **PTN8**, and the blend films were the same as those in solar cell devices. Tapping-mode atomic force microscopy (AFM) images were obtained with a Veeco Multimode V instrument, the Standard Silicon Cantilever AFM tips were from OLYMPUS company with a radius of 10 nm. Transmission electron microscopy (TEM) images and high-angle annular dark-field scanning transmission-electron microscopy (HAADF-STEM) images were obtained by using a Tecnai G2 F20 S-Twin transmission electron microscope. 2D Grazing Incidence X-Ray Diffraction (2D GIXD) experiments were conducted at Shanghai Synchrotron Radiation Facility (SSRF) on a diffraction beamline (BL14B1).

### General procedure for the synthesis of PTN8

In a 50 mL dry reaction tube, 2,6-bis(trimethyltin)-4,8-bis(5-(2-ethylhexyl)thiophen-2-yl)benzo[1,2-*b*:4,5*b*′]dithiophene (0.22 g, 0.24 mmol), 1,3-dibromo-6-hexylnaphtho[2,3-*c*]thiophene-4,9-dione (0.12 g, 0.24 mmol), tri(*o*-tolyl)phosphine (0.02 g, 0.08 mmol), and $Pd_2(dba)_3$ (0.01 g, 0.01 mmol) were dissolved in 5 mL dry toluene under argon. After being stirred at 110 °C for 48 h, the mixture was cooled to room temperature and precipitated in methanol (80 mL). The precipitate was filtered and washed with methanol (24 h) and hexane (24 h) successively in a Soxhlet apparatus to remove oligomers and catalyst residue. Finally, the polymer was extracted with chloroform. The chloroform fraction was concentrated and precipitated in methanol. The precipitate was filtered and dried in vacuum at 80 °C overnight. **PTN8** was obtained as a dark purple solid (200 mg, 87% yield), GPC: $M_n$ = 20.3 kDa,[1] PDI = 2.17; $^1$H NMR (400 MHz, $CDCl_3$): $\delta$ (ppm) 8.70–8.10 (br, 2H ArH), 7.60–6.90 (br, 3H ArH), 3.20–2.50 (br, 6H), 2.00–0.50 (br, 47H).

### Device fabrication and measurements

Polymer solar cells were fabricated with a general structure of ITO/PEDOT-PSS (40 nm)/polymer:$PC_{71}BM$/LiF/Al. Patterned ITO glass substrates were cleaned by sequential ultrasonic treatment in detergent, acetone, deionized water and isopropyl alcohol. The organic residue was further removed by treating with UV-ozone for 10 min. A thin film of PEDOT:PSS (Al 4083, ~40 nm) was spin-coated on ITO substrates and dried at 150 °C for 10 min in air. A blend of polymers and $PC_{71}BM$ with different ratios was dissolved in chloroform containing 0–2% (v/v) diiodooctane (DIO), a fixed polymer concentration of 8 mg $mL^{-1}$ was used for different D/A ratio solutions, DIO content was optimized as 0.5% for D/A weight ratio of 1/0.3 and 1/0.5, 1.0% for 1/0.6 and 1/0.7, 1.5% for 1/0.8 and 2.0% for 1/1.0, filtered through a 0.45 μm poly(tetrafluoroethylene) (PTFE) filter, spin-coated at 1500 rpm for 40 s under an inert atmosphere (with a thickness range from 85 nm to 115 nm), 0.6 nm of LiF (0.2 A $s^{-1}$) and 100 nm Al (2 A $s^{-1}$) layers were then thermally evaporated on the active layer at a pressure of $1.0 \times 10^{-6}$ mbar through a shadow mask (active area 7.25 $mm^2$). The current density–voltage characteristics of the photovoltaic cells were measured using a Keithley 2400 (*I–V*) digital source meter under a simulated AM 1.5G solar irradiation at 100 mW $cm^{-2}$ in a glovebox (Newport, Class AAA solar simulator, 94023A-U). The light intensity is calibrated by using a certified Oriel Reference Cell (91150 V) and verified with a NREL calibrated Hamamatsu S1787-04 diode. The external quantum efficiency (EQE) was performed using a certified IPCE instrument (Zolix Instruments, Inc., SolarCellScan100).

## Acknowledgements

We acknowledge technical support from workers at Shanghai Synchrotron Radiation Facility (SSRF) on diffraction beamline (BL14B1). This work was supported by the National High Technology Research and Development Program of China (863 Program) (Grant No. 2011AA050520), the National Natural Science Foundation of China (Grant No. 61176054), the Natural Science Foundation of Jiangsu Province, China (Grant No. BK2011279), the Doctoral Fund of Ministry of Education of China (Grant No. 20113201120019). J. Yuan thanks State-Sponsored Scholarship for Graduate Students from the China Scholarship Council and the Innovation of Graduate Student Training Project in Jiangsu Province.

## Notes and references

1 (*a*) Y.-J. Cheng, S.-H. Yang and C.-S. Hsu, *Chem. Rev.*, 2009, **109**, 5868–5923; (*b*) W. Wu, Y. Liu and D. Zhu, *Chem. Soc. Rev.*, 2010, **39**, 1489–1502; (*c*) Y. Li, *Acc. Chem. Res.*, 2012, **45**, 723–733; (*d*) H. Zhou, L. Yang and W. You, *Macromolecules*, 2012, **45**, 607–632.

2 (*a*) L. Dou, J. You, J. Yang, C.-C. Chen, Y. He, S. Murase, T. Moriarty, K. Emery, G. Li and Y. Yang, *Nat. Photonics*, 2012, **6**, 180–185; (*b*) Z. He, C. Zhong, S. Su, M. Xu, H. Wu and Y. Cao, *Nat. Photonics*, 2012, **6**, 591–595; (*c*) J. You, L. Dou, K. Yoshimura, T. Kato, K. Ohya, T. Moriarty, K. Emery, C.-C. Chen, J. Gao, G. Li and Y. Yang, *Nat. Commun.*, 2013, **4**, 1446–1456; (*d*) C.-C. Chen, W.-H. Chang, K. Yoshimura, K. Ohya, J. You, J. Gao, Z. Hong and Y. Yang, *Adv. Mater.*, 2014, **26**, 5670–5677.

3 (*a*) S. J. Lou, J. M. Szarko, T. Xu, L. Yu, T. J. Marks and L. X. Chen, *J. Am. Chem. Soc.*, 2011, **133**, 20661–20663; (*b*) Y. Gu, C. Wang and T. P. Russell, *Adv. Energy Mater.*, 2012, **2**, 683–690; (*c*) X. Guo, C. Cui, M. Zhang, L. Huo,

 

Y. Huang, J. Hou and Y. Li, *Energy Environ. Sci.*, 2012, **5**, 7943–7949; (*d*) Y. Sun, G. C. Welch, W. L. Leong, C. J. Takacs, G. C. Bazan and A. J. Heeger, *Nat. Mater.*, 2012, **11**, 44–48.

4 (*a*) J. Peet, J. Y. Kim, N. E. Coates, W. L. Ma, D. Moses, A. J. Heeger and G. C. Bazan, *Nat. Mater.*, 2007, **6**, 497–500; (*b*) J. K. Lee, W. L. Ma, C. J. Brabec, J. S. Moon, J. Y. Kim, K. Lee, G. C. Bazan and A. J. Heeger, *J. Am. Chem. Soc.*, 2008, **130**, 3619–3623; (*c*) J. Yuan, X. Huang, F. Zhang, J. Lu, Z. Zhai, C. Di, Z. Jiang and W. Ma, *J. Mater. Chem.*, 2012, **22**, 22734–22742.

5 (*a*) S. H. Park, A. Roy, S. Beaupré, S. Cho, N. Coates, J. S. Moon, D. Moses, M. Leclerc, K. Lee and A. J. Heeger, *Nat. Photonics*, 2009, **3**, 297–302; (*b*) L. Dou, J. Gao, E. Richard, J. You, C.-C. Chen, K. C. Cha, Y. He, G. Li and Y. Yang, *J. Am. Chem. Soc.*, 2012, **134**, 10071–10079; (*c*) Y.-X. Xu, C.-C. Chueh, H.-L. Yip, F.-Z. Ding, Y.-X. Li, C.-Z. Li, X. Li, W.-C. Chen and A. K. Y. Jen, *Adv. Mater.*, 2012, **24**, 6356–6361; (*d*) D. Qian, W. Ma, Z. Li, X. Guo, S. Zhang, L. Ye, H. Ade, Z. Tan and J. Hou, *J. Am. Chem. Soc.*, 2013, **135**, 8464–8467.

6 (*a*) A. C. Mayer, M. F. Toney, S. R. Scully, J. Rivnay, C. J. Brabec, M. Scharber, M. Koppe, M. Heeney, I. McCulloch and M. D. McGehee, *Adv. Funct. Mater.*, 2009, **19**, 1173–1179; (*b*) N. C. Miller, E. Cho, M. J. N. Junk, R. Gysel, C. Risko, D. Kim, S. Sweetnam, C. E. Miller, L. J. Richter, R. J. Kline, M. Heeney, I. McCulloch, A. Amassian, D. Acevedo-Feliz, C. Knox, M. R. Hansen, D. Dudenko, B. F. Chmelka, M. F. Toney, J.-L. Brédas and M. D. McGehee, *Adv. Mater.*, 2012, **24**, 6071–6079.

7 (*a*) J. Yuan, Z. Zhai, H. Dong, J. Li, Z. Jiang, Y. Li and W. Ma, *Adv. Funct. Mater.*, 2013, **23**, 885–892; (*b*) J. Yuan, H. Dong, M. Li, X. Huang, J. Zhong, Y. Li and W. Ma, *Adv. Mater.*, 2014, **26**, 3624–3630.

8 (*a*) W. Y. Huang, P. T. Huang, Y. K. Han, C. C. Lee, T. L. Hsieh and M. Y. Chang, *Macromolecules*, 2008, **41**, 7485–7489; (*b*) T. Agostinelli, S. Lilliu, J. G. Labram, M. C. Quiles, M. Hampton, E. Pires, J. Rawle, O. Bikondoa, D. D. C. Bradley, T. D. Anthopoulos, J. Nelson and J. E. Macdonald, *Adv. Funct. Mater.*, 2011, **21**, 1701–1708.

9 D. Qian, W. Ma, Z. Li, X. Guo, S. Zhang, L. Ye, H. Ade, Z. Tan and J. Hou, *J. Am. Chem. Soc.*, 2013, **135**, 8464–8467.

10 (*a*) Q. T. Zhang and J. M. Tour, *J. Am. Chem. Soc.*, 1998, **120**, 5355–5362; (*b*) C. Cui, X. Fan, M. Zhang, J. Zhang, J. Min and Y. Li, *Chem. Commun.*, 2011, **47**, 11345–11347.

11 B. Carsten, F. He, H. J. Son, T. Xu and L. Yu, *Chem. Rev.*, 2011, **111**, 1493–1528.

12 (*a*) Y. Zhang, S. K. Hau, H.-L. Yip, Y. Sun, O. Acton and A. K. Y. Jen, *Chem. Mater.*, 2010, **22**, 2696–2698; (*b*) Y. Li, P. Sonar, S. P. Singh, W. Zengb and M. S. Soh, *J. Mater. Chem.*, 2011, **21**, 10829–10835; (*c*) J. Yuan, Z. Zhai, J. Li, J. Lu, X. Huang, Z. Xu and W. Ma, *J. Mater. Chem. A*, 2013, **1**, 12128–12136.

13 (*a*) B. Delley, *J. Phys. Chem.*, 1996, **100**, 6107–6110; (*b*) B. Delley, *J. Chem. Phys.*, 2000, **113**, 7756–7764; (*c*) B. Delley, *J. Chem. Phys.*, 1990, **92**, 508–517; J. Yuan, Y. Zang, H. Dong, G. Liu, C. Di, Y. Li and W. Ma, *Polym. Chem.*, 2013, **4**, 4199–4206.

14 C. Lee, W. Yang and R. G. Parr, *Phys. Rev. B: Condens. Matter*, 1988, **37**, 785–789.

15 J. Andzelm, C. Kölmel and A. Klamt, *J. Chem. Phys.*, 1995, **103**, 9312–9320.

16 S. L. Mayo, B. D. Olafson and W. A. Goddard, *J. Phys. Chem.*, 1990, **94**, 8897–8909.

17 (*a*) J. K. Lee, W. L. Ma, C. J. Brabec, J. S. Moon, J. Y. Kim, K. Lee, G. C. Bazan and A. J. Heeger, *J. Am. Chem. Soc.*, 2008, **130**, 3619–3623; (*b*) S. J. Lou, J. M. Szarko, T. Xu, L. Yu, T. J. Marks and L. X. Chen, *J. Am. Chem. Soc.*, 2011, **133**, 20661–20663; (*c*) X. Guo, C. Cui, M. Zhang, L. Huo, Y. Huang, J. Hou and Y. Li, *Energy Environ. Sci.*, 2012, **5**, 7943–7949; (*d*) Y. Gu, C. Wang and T. P. Russell, *Adv. Energy Mater.*, 2012, **2**, 683–690.

18 (*a*) A. K. K. Kyaw, D. H. Wang, D. Wynands, J. Zhang, T.-Q. Nguyen, G. C. Bazan and A. J. Heeger, *Nano Lett.*, 2013, **13**, 3796–3801; (*b*) A. K. K. Kyaw, D. H. Wang, D. H. V. Gupta, W. L. Leong, L. Ke, G. C. Bazan and A. J. Heeger, *ACS Nano*, 2013, **7**, 4569–4577.